# Investigations on the Interactions between Plasma Proteins and Magnetic Iron Oxide Nanoparticles with Different Surface Modifications

**Shujie Liu, Yuchun Han, Ruirui Qiao, Jianfeng Zeng, Qiaojuan Jia, Yilin Wang,* and Mingyuan Gao***

*Institute of Chemistry, the Chinese Academy of Sciences, Bei Yi Jie 2, Zhong Guan Cun, Beijing 100190, China*

*Received: September 11, 2010; Revised Manuscript Received: October 20, 2010*

Three types of magnetic iron oxide nanoparticles with various kinds of surface modifications were synthesized, and the interactions between the nanoparticles and two types of high abundant plasma proteins were investigated by isothermal titration calorimetry and dynamic light scattering (DLS) methods. It was found that these interactions were strongly dependent on the surface properties of the nanoparticles. Enthalpy−entropy analysis suggested that poly(ethylene glycol) (PEG) modification on the particle surface could effectively reduce the interactions between the magnetic nanoparticles and the plasma proteins. DLS investigations further implied that electrostatic attractions could either increase or decrease the colloidal stability of the nanoparticles, depending on the particle surface properties, which will give rise to different in vivo biodistributions for the intravenously injected nanoparticles, according to literature reports. Proper surface modifications, upon the use of PEG in combination with various types of small molecules for reducing surface charges, were found to be effective for eliminating the strong interactions between nanoparticles and proteins, which is of the utmost importance for developing iron oxide magnetic nanoparticles with long blood circulation time for in vivo applications.

## Introduction

Over the past 10 years, magnetic iron oxide nanoparticles have attracted increasing research interest owing to their applications in biological and biomedical fields.[1−6] With respect to biomedical applications, so far, several kinds of contrast agent-based iron oxide nanoparticles for magnetic resonance (MR) imaging have been commercialized.[1,3,6] Recent investigations further suggest that the magnetic iron oxide nanoparticles are an ideal type of nanomaterial suitable for more sophisticated in vivo applications, such as molecular MR imaging of early tumors.[7−14] The advantages of iron oxide nanoparticles for being used in vivo include their low toxicity in comparison with other types of nanomaterials;[1,15] high sensitivity for MR contrast enhancement owing to their unique superparamagnetism;[16] and multiple surface binding sites, which are essentially required for developing multimodal imaging agents by simultaneously integrating various types of probes,[4,17] although the possession of multiple surface binding sites is a general characteristic for nanomaterials.

Nevertheless, also because of the multiple surface binding sites, as a gift of the large surface-to-volume ratio of nanomaterials, control over the surface properties of nanoparticles remains challenging. With respect to in vivo applications of magnetic iron oxide nanoparticles, the tissue distribution and clearance behavior of nanoparticles are greatly influenced by the opsonization process because the intravenously injected nanoparticles would first be adsorbed by opsonins (i.e., circulating plasma proteins, including various subclasses of immunoglobulins, complement proteins, fibronectin, etc.) and then taken up by the reticuloendothelial system (RES),[18] alternatively known as the mononuclear phagocyte system. Therefore, the inorganic nanoparticles, even with the same core size and chemical composition, may also present quite different biological behaviors due to the differences in surface properties that determine the interactions between the nanoparticles and plasma proteins, leading to different fates and metabolic pathways. Thus, developing proper surface chemistry and further correlating the particle surface properties with the biodistribution behaviors are the most fundamental issues for in vivo applications of magnetic iron oxide nanoparticles, which are also meaningful for clarifying the confusing results in the literature with respect to in vivo applications of nanomaterials.

So far, different solution-based synthetic approaches have been developed for producing iron oxide magnetic nanomaterials with well controllable sizes.[1,3,19] However, in comparison with hydrolytic synthetic routes, the nonhydrolytic synthetic routes are generally more suitable for preparing iron oxide nanoparticles with versatile surface structures by choosing weak polar fatty acids and fatty amines;[20,21] strong polar 2-pyrrolidone;[22,23] and water-soluble macromolecules, such as PEG (poly(ethylene glycol)) as surface capping agents,[24] or using them in different combinations.[9,13,25]

PEG with different molecular weights has widely been used in biomedicine. In addition, it is also a useful type of bioantifouling materials for rendering inorganic nanomaterials biocompatible.[13,24,25] In general, PEG can effectively reduce the interactions between underlying inorganic nanoparticles and plasma proteins so that the agglomeration of the nanoparticles caused by protein adsorption is greatly minimized.[26] Nevertheless, due to the large surface-to-volume ratio for nanomaterials, the surface attachment of PEG does not necessarily exclude additional binding of other molecules.[25] Therefore, iron oxide nanoparticles modified with PEG or PEG in combination with various types of small molecular weight species offers an excellent platform for understanding the interactions between

* To whom correspondence should be addressed. (M.G.) Fax: 86-10-82613214. E-mail: gaomy@iccas.ac.cn. (Y.W.) Fax: 86-10-82615802. E-mail:yilinwang@iccas.ac.cn.

10.1021/jp1086653 
Published on Web 11/16/2010

nanomaterials with plasma proteins, which is essential for understanding the in vivo biodistributions of nanomaterials.

Enlightened by the early works of Sun and his colleagues on the preparations of well-defined magnetic iron oxide particles via the pyrolysis of ferric triacetylacetonate ($Fe(acac)_3$) in diphenyl oxide,[20,21] we developed a facile synthetic route for preparing water-soluble magnetite nanocyrstals upon the use of 2-pyrrolidone instead of diphenyl oxide.[22,23] Further investigations suggest that 2-pyrrolidone not only can provide a high enough reaction temperature but also serves as a coordinating agent to prevent the iron oxide nuclei from uncontrollable growth into bulk material.[23] Benefiting from the excellent mutual solubility with PEG, the 2-pyrrolidone reaction system also allows the preparation of biocompatible magnetite nanocrystals costabilized by PEG terminated with carboxylic acid group(s) and 2-pyrrolidone.[13,25] Very recently, it has been further demonstrated that magnetite nanocrystals simultaneously stabilized by PEG and oleylamine can also be obtained in a nonpolar solvent system.[9] However, the following in vivo experiments reveal that the magnetite nanocrystals costabilized by PEG and 2-pyrrolidone present a superficial long blood circulating behavior and are slowly accumulated in liver after intravenous injection.[24] In contrast, the magnetite nanocrystals costabilized by PEG and oleylamine exhibit quite different biological behaviors. They are distributed quickly in liver after intravenous injection and then slowly washed out, exhibiting a much longer blood half-life. Consequently, the sensitivity in MRI detection of early tumors is dramatically increased due to the effective accumulation of the latter particles mediated by antibody−antigen interaction.[9] To reveal the effects of particle surface properties and understand these behaviors, magnetite nanocrystals stabilized by PEG, costabilized by PEG and 2-pyrrolidone or PEG and oleylamine were prepared for the current study. By isothermal titration calorimetry (ITC) and dynamic light scattering (DLS) methods, the interactions of these iron oxide nanoparticles with bovine serum albumin (BSA) and immunoglobulin G (IgG) were investigated, and the interaction mechanisms are discussed.

## Experimental Section

**Reagents.** Iron(III) acetylacetonate ($Fe(acac)_3$) was purchased from Aldrich (14024-18-1) and used after two recrystallizations. Ethanol, ether, 2-pyrrolidone, and diphenyl oxide of analytical grade were purchased from Sinopharm Chemical Reagent Beijing, Co., Ltd. 2-Pyrrolidone and diphenyl oxide were used after further purification by reduced pressure distillation. Oleylamine was purchased from Fluka (75350) and used as received. BSA was purchased from Amresco (9048-46-8, biotechnology grade). IgG (anti-EGFR) was a gift from the Peking University and used after dialysis. α,ω-Dicarboxyl-terminated PEG 2000 (HOOC-PEG-COOH) was synthesized according to the literature.[24]

**Preparation of $Fe_3O_4$ Nanoparticles with Different Surface Structures.** Three different types of $Fe_3O_4$ nanoparticle samples were prepared according to previous reports and were denoted as samples A, B, and C.

Sample A was magnetite nanocrystals costabilized by PEG and 2-prrrolidone and prepared according to a literature report.[13] Typically, 20 mL of 2-pyrrolidone solution containing $Fe(acac)_3$ (0.1 M) and HOOC-PEG-COOH (0.05 M, $M_n = 2000$) was prepared and purged with nitrogen, then the reaction mixture was heated and kept at 200 °C for 30 min, followed by 1.5 h at 240 °C. After that, the $Fe_3O_4$ nanoparticles were obtained after a set of purifying procedures, including precipitation, magnetic separation, dissolution, and dialysis, as described in previous reports.[13]

Sample B was magnetite nanocrystals costabilized by PEG and oleylamine and prepared according to a previous report.[9] The preparation runs were as follows: Typically, a stock solution of 100 mL of diphenyl oxide containing $Fe(acac)_3$ (0.06 M), HOOC-PEG-COOH (0.12 M, $M_n = 2000$) and oleylamine (0.24 M) was prepared. After being purged with nitrogen for 0.5 h, the reaction mixture was heated to reflux and kept at ∼250 °C for 0.5 h. The reaction was terminated by cooling the reaction mixture to room temperature, followed by slow addition of ether to precipitate the $Fe_3O_4$ nanoparticles which were then magnetically collected with a permanent magnet (0.5 T), which was followed by redissolving the isolated precipitate in ethanol. Typically, this purifying procedure was repeated for three cycles to purify the $Fe_3O_4$ particles, which was followed by dialysis against pure water for 2 days to remove all species with molecular weights smaller than 8000. Finally, the purified particles were dissolved in phosphate buffer saline (PBS) for further experiments.

Sample C was magnetite nanocrystals solely stabilized by PEG. The preparation procedures for sample C were similar to those for sample B except that oleylamine was not presented in the reaction system. Moreover, sample C was obtained after 12 h of reflux. The following purification procedures, including precipitation, magnetic separation, dissolution and dialysis, were the same as those for sample B.

**Isothermal Titration Calorimetry Measurements.** All ITC measurements were performed with the aid of a microcalorimetric system equipped with a 1 mL stainless steel sample cell maintained at 298.15 ± 0.01 K. The sample cell was first loaded with 0.7 mL particle solution (0.1 mg/mL in PBS), then 8 μL of protein solution of BSA or IgG with a concentration of 3 mg/mL in PBS was injected into the sample cell by a microsyringe under stirring using a gold propeller (50 rpm). A series of injections were accomplished until a desired concentration range was reached. Meanwhile, the heat flow was recorded and plotted against time $t$ after each injection. By subtracting the heat flow caused by protein dilution, the observed enthalpy changes ($\Delta H_{obs}$) was obtained by integrating the heat flow. All experiments were repeated, and the reproducibility was within ±4%. By fitting the observed enthalpy curves plotted against the molar ratio of protein to particle, the binding constants ($K_b$) and the enthalpy changes ($\Delta H$) were derived. The free energy changes ($\Delta G$) were calculated from $\Delta G = -RT \ln K_b$, and the entropy changes were from $T\Delta S = \Delta H - \Delta G$.

**Dynamic Light-Scattering Measurements.** DLS investigations were performed to further reveal the colloidal stability of nanoparticles in the absence or presence of proteins in PBS buffer. The molar ratio of $Fe_3O_4$/BSA was set to 1:83; that of $Fe_3O_4$/IgG was set to 1:32 according to the ITC measurements by choosing the molar ratios by which the saturated surface adsorption of proteins, if they exist, are not reached yet. The DLS results are expressed by scattering intensity versus hydrodynamic size so as to better present the aggregates appearing in the systems because the intensity of the scattering of a particle is proportional to the sixth power of its diameter from Rayleigh's approximation.

**Characterizations.** All $Fe_3O_4$ nanoparticle samples were characterized by transmission electron microscope (TEM) (JEM-100CXII) operating at an accelerating voltage of 100 kV. The organic content in each sample was estimated by thermogravimetry analysis (TGA, EXSTAR 6000, TG/DTA 6300) in com-

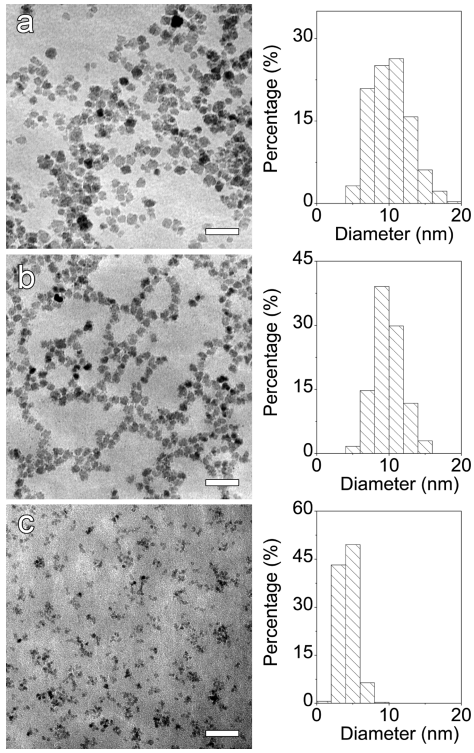


**Figure 1.** TEM images and the corresponding particle size histograms of sample A (a), sample B (b), and sample C (c). The scale bars represent 50 nm.

bination with X-ray photoelectron spectroscopy (XPS). The temperature was increased by a rate of 10 °C/min for all TGA measurements. The upper limit was set to 600 °C. X-ray photoelectron spectroscopy (XPS) measurements were performed with an ESCALAB 220i-XL photoelectron spectrometer from VG Scientific using 300 W Mg Kα radiation ($h\nu = 1253.6$ eV). ITC measurements were carried out on a TAM 2277-201 microcalorimetric system (Thermometric AB, Järfälla, Sweden) equipped with a 500 $\mu$L Hamilton syringe controlled by a 612 Thermometric Lund pump for sample injection. DLS measurements were carried out at 298.0 K with a Nano ZS (Malvern) equipped with a solid-state He−Ne laser ($\lambda = 633$ nm) for monitoring the changes in the hydrodynamic size of particles upon their interactions with proteins.

## Results and Discussion

**1. Magnetic Nanoparticles with Different Surface Structures.** The magnetic nanoparticles were first characterized by TEM. Three representative TEM images of samples A, B, and C together with the corresponding particle size histograms are shown in Figure 1. The average size is 10.2 nm for sample A, 9.9 nm for sample B, and 4.4 nm for sample C. The particle sizes of samples A and B are quite comparable, but larger than that of sample C, indicating that small molecules can effectively regulate the particle growth. Although the particle samples with comparable particle sizes are ideal for the following experiments, PEG seems to have a strong ability to prevent the magnetite nanocrsytals from growing bigger due to its strong interactions with iron oxide nanoparticles, which also explains that in the absence of small addictives, it is very difficult to obtain magnetite nanocrystals larger than 5 nm by using α,ω-dicarboxyl-terminated PEG as a particle surface capping agent.

To further investigate the surface compositions of samples A, B, and C, TGA measurements were first carried out, and the

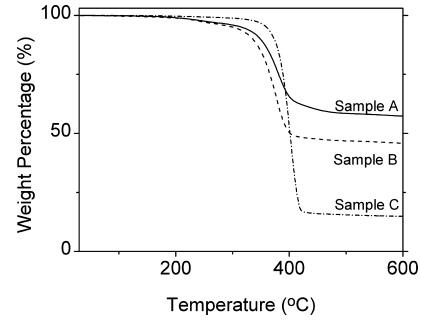


**Figure 2.** TGA curves of samples A (—), sample B (- - - -), and sample C (−•−•−).

results were analyzed in combination with XPS results. The TGA curves for samples A, B, and C are shown in Figure 2. It is quite obvious that in addition to a smaller size, sample C also has the highest organic content due to the surface modification by pure PEG. The final organic content is 42.7% for sample A, 53.2% for sample B, and 85.1% for sample C.

The XPS measurements revealed that both sample A and sample B contain nitrogen, which comes from 2-pyrrolidone for sample A and oleylamine for sample B, respectively. The atomic contents of N and C in sample A were 4.16% and 56.04%, and those in sample B were 1.56% and 75.91%, respectively. On the basis of these data, the molar ratio between PEG and 2-pyrrolidone in sample A was calculated to be 1:9.50. Similarly, the molar ratio of PEG to oleylamine was calculated to be 1:2.94. Further in combination with the TGA results, the molar ratios of PEG/$Fe_3O_4$ were calculated to be 0.062:1, 0.097:1, and 0.656:1 for samples A, B, and C, respectively. In fact, it is not difficult to understand the sequence of the PEG/$Fe_3O_4$ ratio in these samples. Because no small-molecular-weight molecules were present in the reaction system generating sample C, it presents the highest PEG/$Fe_3O_4$ ratio. Although sample A was prepared in 2-pyrrolidone, it presents the lowest PEG/$Fe_3O_4$ ratio because 2-pyrrolidone, as a coordinating solvent, was in great excess in the reaction system.

The PEG/$Fe_3O_4$ ratio to some extent can be taken as an indicator for stabilization degree provided by PEG for the underlying iron oxide nanocrystals. Nevertheless, the simultaneous modification of PEG in combination with oleylamine or 2-pyrrolidone not only affects the particle size, the PEG modification degree, but it will also dramatically alter the solution properties of the resultant nanoparticles. As a matter of fact, the surface coordination of 2-pyrrolidone is not effective enough to prevent the underlying magnetite nanocrystals from protonation or deprotonation, which can find support from the facts that the magnetic nanocrystals solely stabilized by 2-pyrrolidone are not dissolved or dispersible in water in neutral pH range, but become dispersible in aqueous solution in both the acidic and alkaline ranges.[23]

Although the aqueous solubility at neutral pH is greatly improved by partly coating the magnetite nanocrystals with PEG, sample A still presents a positive zeta potential of +22.9 mV. In contrast, the zeta potential of sample B, which consists of magnetite nanocrystals costabilized by PEG and oleylamine, is reversed to slightly negative, −2.1 mV, partly due to the existence of carboxylic residues on the particle surface, which further implies that oleylamine can firmly stick to the particle surface and prevent the particle core from protonation or deprotonation. In addition, oleylamine provides a certain degree of hydrophobicity to the nanoparticles, which makes the resultant particles more like a protein. With respect to sample C, the zeta

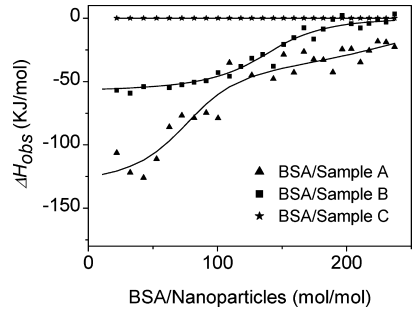


**Figure 3.** ITC curves recorded during the addition of BSA into PBS solutions of samples A (▲), B (■), and C (★) at 25 °C. The solid lines represent the best fittings.

**TABLE I: Binding Constants ($K_b$), Gibbs Free Energy Changes ($\Delta G$), Enthalpy Changes ($\Delta H$), and Entropy Changes ($T\Delta S$) for the Samples A−C in Interaction with BSA in PBS (pH 7.4) at 25°C[a]**

| | $K_b$ ($M^{-1}$) | $\Delta G$ (kJ·mol$^{-1}$) | $\Delta H$ (kJ·mol$^{-1}$) | $T\Delta S$ (kJ·mol$^{-1}$) |
|---|---|---|---|---|
| sample A | $3.20 \times 10^7$ | −42.91 | −129.60 | −86.67 |
| | $7.93 \times 10^5$ | −32.09 | −42.98 | −10.89 |
| sample B | $2.98 \times 10^6$ | −36.95 | −58.44 | −21.48 |
| sample C | ∼0 | ∼0 | ∼0 | ∼0 |

[a] The ITC curve of BSA/sample A was fitted by two sets of independent sites; for more details see the Supporting Information.

potential is more negative, −19.9 mV, because there are more carboxylic residues from α,ω-dicarboxyl-terminated PEG rooting from the particle surface. All these three samples present excellent colloidal stability in pure water, but in PBS buffer, the colloidal stability of sample A is greatly reduced. Typically, after 24 h, most particles were precipitated, as shown in Figure S1 in the Supporting Information (SI). In contrast, samples B and C presented very good colloidal stability in PBS buffer, as shown in Figures S2 and S3 in the Supporting Information.

**2. Interactions between BSA and Iron Oxide Nanoparticles.** Serum albumin is the most abundant plasma protein in mammals, so their interaction with nanoparticles intravenously injected greatly affects in vivo biodistribution of the nanoparticles.[27] In the current investigations, BSA was chosen as a model SA protein for investigating its interactions with iron oxide nanoparticles with different surface structures and properties. The ITC curves in Figure 3 show that samples A, B, and C have distinctly different enthalpy change profiles in interacting with BSA. The interactions of samples A and B with BSA are exothermic processes, whereas sample C exhibits nearly no interactions with BSA. The ITC curves were analyzed by standard Marquardt methods with an ITC package (supplied by Microcal Inc.) embedded in the Origin program to further extract the binding constant, $K_b$, and enthalpy changes, $\Delta H$, then $\Delta G$ and $T\Delta S$ were derived. The detailed results are tabulated in Table I.

In fact, the ITC curve of BSA/sample A was barely fitted by the model of a single set of identical sites, indicating that there exists more than one distinct process in the BSA/sample A complexation. It was further confirmed that the ITC curve for BSA/sample A can satisfactorily be fitted by two sets of independent sites models. In contrast, the observed enthalpy changes for BSA/sample C are quite close to zero within the observation range, suggesting that there are nearly no interactions between BSA and sample C. The resultant binding constants of BSA with samples A, B, and C were $3.20 \times 10^7$, $2.98 \times 10^6$, and ∼0 $M^{-1}$, respectively, leading to a binding strength sequence of sample A > sample B > sample C.

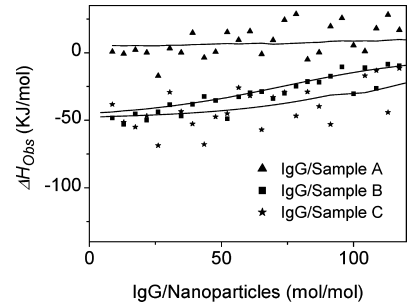


**Figure 4.** ITC curves recorded during the addition of IgG into PBS solutions of samples A (solid triangle), B (solid square), and C (solid star) at 25 °C. The solid lines represent the best fittings.

**TABLE II: Binding Constants ($K_b$), Gibbs Free Energy Changes ($\Delta G$), Enthalpy Changes ($\Delta H$), and Entropy Changes ($T\Delta S$) for the Samples A−C in Interaction with IgG in PBS (pH 7.4) at 25°C**

| | $K_b$ ($M^{-1}$) | $\Delta G$ (kJ·mol$^{-1}$) | $\Delta H$ (kJ·mol$^{-1}$) | $T\Delta S$ (kJ·mol$^{-1}$) |
|---|---|---|---|---|
| sample A | ∼0 | ∼0 | ∼0 | ∼0 |
| sample B | $1.44 \times 10^6$ | −35.15 | −50.86 | −15.71 |
| sample C | $2.61 \times 10^6$ | −36.62 | −50.19 | −13.57 |

In fact, the interactions between BSA and iron oxide nanoparticles may involve electrostatic interaction, hydrogen bonding, and hydrophobic−hydrophobic interaction, depending on the particle surface chemical structure and surface physical properties. In the case of sample A, $\Delta H$ is the highest among all samples, reaching −129 kJ·mol$^{-1}$, which indicates that electrostatic interactions are involved. This can easily be understood. Because the isoelectric point of BSA is around 4.7, BSA is therefore negatively charged in PBS buffer; but around neutral pH, sample A is positively charged, as mentioned above. With respect to sample B, the magnetite nanoparticles are stabilized by PEG and hydrophobic oleylamine. The effective surface modification by oleylamine greatly reduces the protonation probability of the underlying particles, in addition to offering a certain degree of hydrophobicity. As a side effect, the amount of PEG on the particle surface is also increased. These overall surface structural differences will undoubtedly be helpful for suppressing the electrostatic attraction between BSA and the magnetic nanoparticles, which is also supported by ITC results. Both the interactions of BSA with sample A and sample B are enthalpy-controlled; however, in comparison with sample A, sample B presents decreased $\Delta H$ and $\Delta S$ values, which can partly be attributed to the decreased electrostatic attraction between BSA and sample B. But $T\Delta S$ decreases more heavily than $\Delta H$; that is, the negative entropy becomes more unfavorable, suggesting that the hydrophobic interaction instead of electrostatic interactions becomes significant for the interactions between BSA and sample B. In contrast, BSA presents nearly no interactions with sample C, which can be attributed to that the nanoparticles in sample C are negatively charged, as is BSA.

**3. Interactions between IgG and Iron Oxide Nanoparticles.** As previously mentioned, IgG plays a very important role in the opsonization process, which is strongly related to the blood circulation behavior of intravenously injected nanoparticles.[18,27] The ITC curves shown in Figure 4 reveal that sample A has very weak interactions with IgG, whereas samples B and C are exothermic in their interactions with BSA. The thermodynamic parameters extracted by fitting the ITC curves shown in Figure 4 are presented in Table II.

Because the observed enthalpy changes ($\Delta H_{obs}$) for sample A fluctuate around zero, so it is concluded that the nanoparticles

in sample A barely interact with IgG, and the binding constant can roughly be taken as zero. The binding constants of samples B and C with IgG were of $1.44 \times 10^6$, and $2.61 \times 10^6$ $M^{-1}$, respectively, extracted by fitting the ITC curves according to the procedures mentioned above. So the binding strength is in a sequence of sample A < sample B < sample C.

According to the zeta potential measurements, sample A is positively charged, and IgG at pH 7.4 is also positively charged because its pI is around 8.1. Therefore, it is reasonably to speculate that the electrostatic repulsion between the nanoparticles of sample A and IgG can effectively prevent IgG molecules from binding with the particles. With respect to sample B, the hydrophobic interaction should still play an important role in the interactions between IgG and nanoparticles, but with a smaller $K_b$ than that of BSA/sample B. Although $\Delta H$ and $\Delta S$ of sample C are slightly smaller than those of sample B, the binding constant is slightly higher than that of sample B, which can be attributed to the electrostatic attraction because sample C is negatively charged at pH 7.4. Nevertheless, the $K_b$ of IgG/sample C is 1 order of magnitude lower than the BSA/sample A system in which electrostatic attraction plays a determined role, which can be attributed to the bioantifouling properties of PEG due to its hindering effect.

**4. DLS Investigations on the Interactions between Proteins and Iron Oxide Nanoparticles.** Even though it remains difficult to fully understand the ITC experimental results due to the complexity of the system consisting of nanoparticles and proteins, the ITC experiments still provide quantitative information on the interactions between nanoparticles with proteins.[28,29] To further discover the effects of the interactions between the nanoparticles and proteins, the DLS method was employed to monitor the evolution of the hydrodynamic size of the nanoparticles in the presence of proteins.

As previously mentioned, the nanoparticles in sample A tended to agglomerate in PBS and largely precipitated out of the solution in 24 h. Such colloidal instability behaviors are clearly reflected in the DLS results shown in Figure 5. In the first couple of hours, the nanoparticles aggregate, forming larger particles that gradually grow in size within the first 4 h. Then, within 24 h, the size of the particle aggregates quickly increases and eventually leads to the formation of larger agglomerates with 3 distinct sizes. Meanwhile, a large percentage of the particles are precipitated out of the solution, as shown in Figure S1 of the Supporting Information. In addition, the nanoparticles also present quite comparable colloidal instability behaviors in the presence of IgG, which further supports that sample A presents nearly no interactions with IgG, as indicated by the ITC experiments.

In contrast, the nanoparticles also tend to grow larger in the presence of BSA, but only with the number-weighted mean hydrodynamic size increasing from 27.4 to 47.8 nm and the intensity-weighted mean hydrodynamic size increasing from 52.6 to 130.3 nm within 24 h. The increased colloidal stability of sample A in the presence of BSA, together with the relatively limited increases in hydrodynamic size, suggest that the electrostatic attraction helps the iron oxide nanoparticles to be more stably dispersed by attaching BSA onto the particle surface (Figure S1 of the Supporting Information). Therefore, it becomes quite understandable for the biodistribution of sample A, which is gradually accumulated in liver after being intravenously injected,[24] because the surface attachment of plasma protein in general facilitates the uptake by liver macrophages.[27]

Different from sample A, the nanoparticles in sample B exhibit much weaker interactions with either BSA or IgG, quite

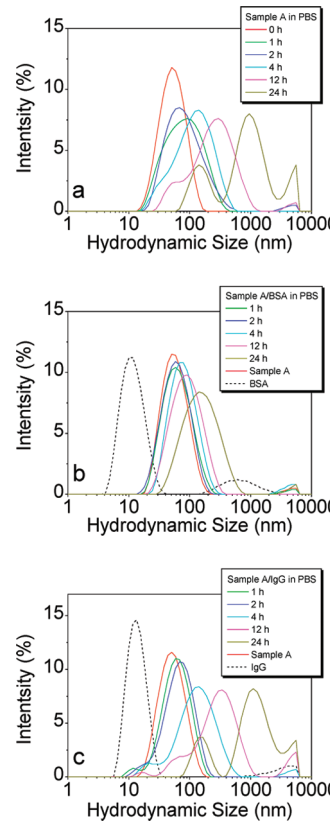


**Figure 5.** Hydrodynamic size profiles of sample A (a), sample A in the presence of BSA (b), or IgG (c) recorded after the solutions were incubated at room temperature for different periods of time.

probably upon hydrophobic interactions and hydrogen bonding, as suggested by the ITC analysis. Moreover, they are more colloidally stable in PBS buffer. Even in the presences of IgG or BSA, the nanoparticles present a nearly unchanged hydrodynamic size profile in comparison with those in PBS buffer, as shown in Figure 6. Consequently, the plasma protein-mediated uptake of sample B by liver macrophages is greatly suppressed, as demonstrated previously, leading to a greatly enhanced blood circulating ability for the iron oxide nanoparticles simultaneously stabilized by both PEG and oleylamine.[9]

It is commonly accepted that PEGylated nanoparticles can avoid the clearance by the RES because PEG can prevent the plasma proteins from being glued onto the particle surface. Even though sample C has the highest PEG content among all three samples, it still presents a certain degree of colloidal instability in the presence of IgG, as shown in Figure 7, which is probably caused by IgG adsorption due to its negative zeta potential. Nevertheless, the negative potential of sample C arises from the surface carboxylic residues from α,ω-dicarboxyl-terminated PEG. Therefore, the interactions between sample C and partly protonated IgG still exhibit different effects on the colloidal stability of the iron oxide nanoparticles if compared with those between sample A and BSA. In the latter case, the colloidal stability of sample A is increased rather than decreased, as shown in Figure 5b, due to the fact that proteins generally have some binding affinities to metal ions.

## Summary

Three types of magnetic iron oxide nanoparticles were prepared by modifying the magnetite nanocrystal cores with 2-pyrrolidone/PEG, oleylamine/PEG, and PEG, respectively. The fine-tuning of the surface modification was achieved by

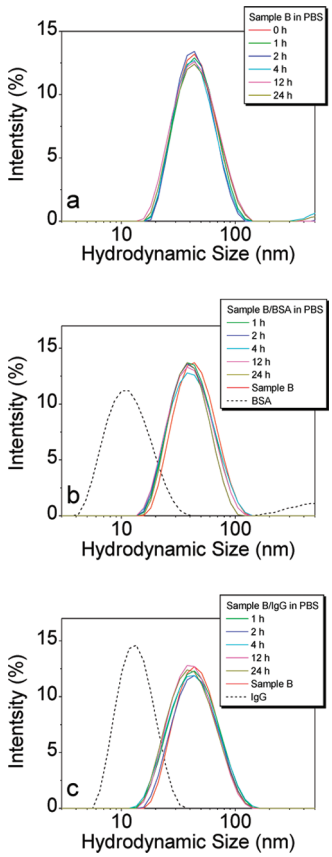


**Figure 6.** Hydrodynamic size profiles of sample B (a), sample B in the presence of BSA (b), or IgG (c) recorded after the solutions were incubated at room temperature for different periods of time.

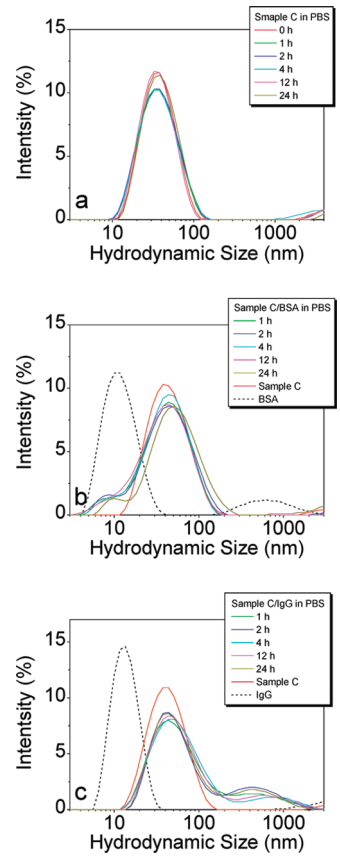


**Figure 7.** Hydrodynamic size profiles of sample C (a), sample C in the presence of BSA (b), or IgG (c) recorded after the solutions were incubated at room temperature for different periods of time.

using different recipes in different solvent systems. Although the resultant nanocrystal cores differ slightly in size, they still allow further ITC measurements for quantitatively estimating the interactions between the nanoparticles with different surface properties and two types of high-abundance proteins in blood serum; that is, SA and IgG. Detailed analysis of ITC experimental results, in combination with DLS investigations, suggest that the protonation of the iron oxide core leads to strong BSA adsorption. Although it helps to improve the colloidal stability of the particles, such plasma protein adsorption will eventually deliver the nanoparticles to the liver upon opsonizaiton effect, as previously demonstrated. Despite the stealth properties of PEGylated particles, with the current synthetic protocol, it remains difficult to achieve adequate leeway for tuning the magnetite core size by pyrolyzing $Fe(acac)_3$ in the presence of carboxyl-terminated PEG in diphenyl oxide.

An alternative approach for obtaining stealth particles is herein achieved by costabilizing the iron oxide nanocrystals with PEG and oleylamine for overcoming the size tuning limit. Such a combination of surface stabilizing agents on one hand will enable the particles to be tuned from 5 to 18 nm (to be published elsewhere) and on the other hand greatly reduce the interactions between plasma proteins and the nanoparticles. Consequently, the resultant magnetic iron oxide nanoparticles costabilized by PEG and olyelamine present the best colloidal stability, irrespective of the presence of BSA or IgG, among all three nanoparticle samples investigated. We believe the current investigations will pave a new route for achieving inorganic nanoparticles with improved stealth properties that are needed for nanoparticles to be used as molecular imaging agents. Further results on iron oxide nanoparticles solely stabilized by α,ω-dicarboxyl-terminated PEG, however, suggest that despite PEG coating, carboxylic residues on the particle surface can still give rise to plasma protein adsorption, leading to colloidal instability. Therefore, it can generally be concluded that PEGylated nanoparticles with an uncharged surface are very important for preparing stealth nanoparticles, and a proper balance between hydrophilic and hydrophobic surface capping agents is also greatly helpful for avoiding the RES clearance of the nanoparticles intravenously injected due to the dramatically reduced protein adsorption.

**Acknowledgment.** The current investigations are jointly supported by a project CAS project (KJCX2-YW-M15), NSFC projects (20820102035, 21003135), and a MOST project (2007AA02Z467).

**Supporting Information Available:** The contents of the Supporting Information include the following experimental details: (1) details of the ITC analysis and (2) photographs of samples A−C in PBS buffer in the absence or presence of proteins. This material is available free of charge via the Internet at http://pubs.acs.org.

## References and Notes

(1) Qiao, R. R.; Yang, C. H.; Gao, M. Y. *J. Mater. Chem.* **2009**, *19*, 6274.
(2) Sun, C.; Lee, J. S. H.; Zhang, M. Q. *Adv. Drug Delivery Rev.* **2008**, *60*, 1252.
(3) Laurent, S.; Forge, D.; Port, M.; Roch, A.; Robic, C.; Vander Elst, L.; Muller, R. N. *Chem. Rev.* **2008**, *108*, 2064.
(4) Jun, Y. W.; Lee, J. H.; Cheon, J. *Angew. Chem., Int. Ed.* **2008**, *47*, 5122.

(5) Gupta, A. K.; Naregalkar, R. R.; Vaidya, V. D.; Gupta, M. *Nanomedicine* **2007**, *2*, 23.
(6) Corot, C.; Robert, P.; Idee, J. M.; Port, M. *Adv. Drug Delivery Rev.* **2006**, *58*, 1471.
(7) Yang, L.; Mao, H.; Cao, Z. H.; Wang, Y. A.; Peng, X. H.; Wang, X. X.; Sajja, H. K.; Wang, L. Y.; Duan, H. W.; Ni, C. C.; Staley, C. A.; Wood, W. C.; Gao, X. H.; Nie, S. M. *Gastroenterology* **2009**, *136*, 1514.
(8) Veiseh, O.; Sun, C.; Fang, C.; Bhattarai, N.; Gunn, J.; Kievit, F.; Du, K.; Pullar, B.; Lee, D.; Ellenbogen, R. G.; Olson, J.; Zhang, M. Q. *Cancer Res.* **2009**, *69*, 6200.
(9) Liu, S. J.; Jia, B.; Qiao, R. R.; Yang, Z.; Yu, Z. L.; Liu, Z. F.; Liu, K.; Shi, J. Y.; Han, O. Y.; Wang, F.; Gao, M. Y. *Mol. Pharm.* **2009**, *6*, 1074.
(10) Xie, J.; Chen, K.; Lee, H. Y.; Xu, C. J.; Hsu, A. R.; Peng, S.; Chen, X. Y.; Sun, S. H. *J. Am. Chem. Soc.* **2008**, *130*, 7542.
(11) Sun, C.; Veiseh, O.; Gunn, J.; Fang, C.; Hansen, S.; Lee, D.; Sze, R.; Ellenbogen, R. G.; Olson, J.; Zhang, M. *Small* **2008**, *4*, 372.
(12) Lee, J. H.; Huh, Y. M.; Jun, Y.; Seo, J.; Jang, J.; Song, H. T.; Kim, S.; Cho, E. J.; Yoon, H. G.; Suh, J. S.; Cheon, J. *Nat. Med.* **2007**, *13*, 95.
(13) Hu, F. Q.; Wei, L.; Zhou, Z.; Ran, Y. L.; Li, Z.; Gao, M. Y. *Adv. Mater.* **2006**, *18*, 2553.
(14) Huh, Y. M.; Jun, Y. W.; Song, H. T.; Kim, S.; Choi, J. S.; Lee, J. H.; Yoon, S.; Kim, K. S.; Shin, J. S.; Suh, J. S.; Cheon, J. *J. Am. Chem. Soc.* **2005**, *127*, 12387.
(15) Tromsdorf, U. I.; Bruns, O. T.; Salmen, S. C.; Beisiegel, U.; Weller, H. *Nano Lett.* **2009**, *9*, 4434.
(16) Jun, Y. W.; Seo, J. W.; Cheon, A. *Acc. Chem. Res.* **2008**, *41*, 179.
(17) Cheon, J.; Lee, J.-H. *Acc. Chem. Res.* **2008**, *41*, 1630.
(18) Moghimi, S. M.; Hunter, A. C.; Murray, J. C. *Pharmacol. Rev.* **2001**, *53*, 283.
(19) Lu, X. Y.; Niu, M.; Qiao, R. R.; Gao, M. Y. *J. Phys. Chem. B* **2008**, *112*, 14390.
(20) Sun, S. H.; Zeng, H.; Robinson, D. B.; Raoux, S.; Rice, P. M.; Wang, S. X.; Li, G. X. *J. Am. Chem. Soc.* **2004**, *126*, 273.
(21) Sun, S. H.; Zeng, H. *J. Am. Chem. Soc.* **2002**, *124*, 8204.
(22) Li, Z.; Sun, Q.; Gao, M. Y. *Angew. Chem., Int. Ed.* **2005**, *44*, 123.
(23) Li, Z.; Chen, H.; Bao, H. B.; Gao, M. Y. *Chem. Mater.* **2004**, *16*, 1391.
(24) Li, Z.; Wei, L.; Gao, M. Y.; Lei, H. *Adv. Mater.* **2005**, *17*, 1001.
(25) Hu, F. Q.; Li, Z.; Tu, C. F.; Gao, M. Y. *J. Colloid Interface Sci.* **2007**, *311*, 469.
(26) Xie, J.; Xu, C. J.; Kohler, N.; Hou, Y. L.; Sun, S. H.; *Adv. Mater.* **2007**, *19*, 3163.
(27) Aggarwal, P.; Hall, J. B.; McLeland, C. B.; Dobrovolskaia, M. A.; McNeil, S. E. *Adv. Drug Delivery Rev.* **2009**, *61*, 428.
(28) De, M.; You, C. C.; Srivastava, S.; Rotello, V. M. *J. Am. Chem. Soc.* **2007**, *129*, 10747.
(29) Cedervall, T.; Lynch, I.; Lindman, S.; Berggard, T.; Thulin, E.; Nilsson, H.; Dawson, K. A.; Linse, S. *Proc. Natl. Acad. Sci. U.S.A.* **2007**, *104*, 2050.

JP1086653